J|A|C|S ARTICLES

Published on Web 05/22/2009

Hydrogen-Promoted Oxygen Activation by Free Gold Cluster Cations

Sandra M. Lang,[†] Thorsten M. Bernhardt,*[,†] Robert N. Barnett,[‡] Bokwon Yoon,[‡] and Uzi Landman*[,‡]

Institute for Surface Chemistry and Catalysis, University of Ulm, Albert-Einstein-Allee 47, 89069 Ulm, Germany, and School of Physics, Georgia Institute of Technology, Atlanta, Georgia 30332-0430

Received March 21, 2009; E-mail: thorsten.bernhardt@uni-ulm.de; uzi.landman@physics.gatech.edu

Abstract: Small gas-phase gold cluster cations are essentially inert toward molecular oxygen. Preadsorption of molecular hydrogen, however, is found to cooperatively activate the binding of O_2 to even-size Au_x^+ ($x = 2, 4, 6$) clusters. Measured temperature- and reaction-time-dependent ion intensities, obtained by ion trap mass spectrometry, in conjunction with first-principles density-functional theory calculations, reveal promotion and activation of molecular oxygen by preadsorbed hydrogen. These processes lead to the formation of a hydroperoxo intermediate on Au_4^+ and Au_6^+ and culminate in the dissociation of O_2 via the release of H_2O. Langmuir−Hinshelwood reaction mechanisms involving the coadsorption of both of the reactant molecules are discussed for both cluster sizes, and an alternative Eley−Rideal mechanism involving hydrogen molecules adsorbed on a Au_6^+ cluster reacting with an impinging gaseous oxygen molecule is analyzed. Structural fluctionality of the gold hexamer cation, induced by the adsorption of hydrogen molecules, and resulting in structural isomerization from a ground-state triangular structure to an incomplete hexagonal one, is theoretically predicted. Bonding of H_2 on cationic gold clusters is shown to involve charge transfer to the clusters. This serves to promote the bonding of coadsorbed oxygen through occupation of the antibonding $2\pi^*$ orbitals, resulting in excess electronic charge accumulation on the adsorbed molecule and weakening of the O−O bond. The theoretical results for hydrogen saturation coverages and reaction characteristics between the coadsorbed hydrogen and oxygen molecules are found to agree with the experimental findings. The joint investigations provide insights regarding hydrogen and oxygen cooperative adsorption effects and consequent reaction mechanisms.

1. Introduction

The catalytic properties of gold particles that emerge when their dimensions are reduced to the nanoscale continue to be a subject of great research interest and an area of discovery.[1−5] Studies of catalysis by gold nanoclusters are part of the fast-developing field of nanocatalysis[4] where emphasis is placed on new size-dependent chemical reactivity and catalytic properties that are found when the size of metal catalyst particles reaches the ultimate nanocluster regime, that is, clusters comprised of up to 10 or 20 atoms, characterized by sizes of up to 1 nm[2,5,6] (see also the discussion in ref 7). Indeed, in this size regime "small is different" [8] in an essential manner that could not have been anticipated through extrapolation of knowledge obtained for larger sizes, and where scaling arguments do not apply. In this nonscalable size regime material aggregates may be regarded as "zero-dimensional" quantum dots whose physical and chemical properties are determined by quantum size effects that originate from the spatial confinement of the electrons. In such nanoclusters a dominant fraction of the atoms are undercoordinated (that is, they are situated in a nonbulk environment), and thus, they are expected to exhibit enhanced chemical reactivity. Furthermore, as commonly found in molecular systems, nanoscale clusters may exhibit a number of structural isomers, and transformations from one isomeric form to another may be induced thermally or chemically (i.e., due to the influence of adsorbates and/or interactions with reactant molecules); such structural effects play an important role in nanocatalysis, and they have been termed "dynamical fluctionality", describing structural variations that may occur in the course of chemical reactions.[9] As a consequence of the above discussion we conclude that to elucidate and understand the electronic and structural factors that control nanocatalytic activity one must focus on experimental and theoretical investigations that highlight the size-dependent correlations between

[†] University of Ulm.
[‡] Georgia Institute of Technology.

(1) Valden, M.; Lai, X.; Goodman, D. W. *Science* **1998**, *281*, 1647.
(2) Sanchez, A.; Abbet, S.; Heiz, U.; Schneider, W.-D.; Häkkinen, H.; Barnett, R. N.; Landman, U. *J. Phys. Chem. A* **1999**, *103*, 9573–9578.
(3) Haruta, M. *Nature* **2005**, *437*, 1098.
(4) *Nanocatalysis*; Heiz, U., Landman, U., Eds.; Springer-Verlag: Berlin, 2007.
(5) Landman, U.; Yoon, B.; Zhang, C.; Heiz, U.; Arenz, M. *Top. Catal.* **2007**, *44*, 145.
(6) Herzing, A. A.; Kiely, C. J.; Carley, A. F.; Landon, P.; Hutchings, G. J. *Science* **2008**, *321*, 1331.
(7) Harding, C.; Habibpour, V.; Kunz, S.; Farnbacher, A. N.-S.; Heiz, U.; Yoon, B.; Landman, U. *J. Am. Chem. Soc.* **2009**, *131*, 538.
(8) Landman, U. *Proc. Natl. Acad. Sci. U.S.A.* **2005**, *102*, 6671.
(9) Häkkinen, H.; Abbet, S.; Sanchez, A.; Heiz, U.; Landman, U. *Angew. Chem., Int. Ed.* **2003**, *42*, 1297.

10.1021/ja9022368 CCC: $40.75 © 2009 American Chemical Society

the electronic structure and geometrical arrangement of the atoms (including dynamic fluctional distortions).

During the past decade it has been found through experimental and theoretical investigations (performed mostly on clusters supported on the surfaces of metal oxides) that the chemical properties and catalytic activity of gold depend on, and can be controlled by, several factors,[2,5,10] including: (i) the size and dimensionality of the gold nanoclusters, (ii) the chemical identity (composition) and structure of the supporting substrate (crystalline or amorphous, surface crystallography, film thickness,[7,11] and degree of perfection, i.e., the presence, or absence, of surface defects, commonly F-center oxygen vacancies), and (iii) the charge state of the catalytic metal cluster,[2,12,13] which may depend on the nature and properties of the support (with charging by electrons originating from surface F-centers playing an important role in the case of supported clusters). These studies have revealed that in heterogeneous catalysis the support (most commonly a metal oxide surface) is often an integral active part of the catalytic system and that the catalytic activity may be controlled through substrate manipulations (for a most recent study see ref 7).

A significant number of recent investigations focused on gold-based oxidation nanocatalysts, which can be operated at low temperatures and are able to efficiently activate molecular oxygen;[2,3,5,7,9,10,12] these properties are of special importance for the development of environmentally sustainable catalytic processes. While the partial oxidation of hydrocarbons is characterized by remarkably high product selectivity, the application of gold particle catalysts is hampered by a poor yield of such processes and by the need to supply equimolar amounts of hydrogen in addition to molecular oxygen.[14] Despite the great interest in this reaction, the role of hydrogen in the oxidation reaction mechanism is largely not understood.[15,16]

Most explorations pertaining to catalysis by gold focused on surface-supported gold catalysts.[1−5] As aforementioned, in these investigations the influence of the substrate support plays an important role in controlling the catalytic activity, and consequently, the observed reactivity consists of a convolution of the gold cluster and support properties. Therefore, to interrogate the intrinsic chemical reactivity of gold nanocluster catalysts (in addition to our long-standing interest in gas-phase nanocluster catalysis), we focus here on free, gas-phase, gold clusters. Previous experimental studies of the reactions of free gold clusters with molecular oxygen revealed that the reactivity of anionic Au_x^- ($x \geq 1$) clusters exhibits a pronounced odd−even alternation, with even-size clusters being reactive while odd-size clusters were found to be essentially inert.[17−19] Such odd−even alternations were also found in theoretical investigations.[20,21] Theoretical calculations also predict binding of O_2 to cluster cations Au_x^+.[22] However, oxidation products of cationic gold clusters (containing, most likely, atomic oxygen) have only been observed experimentally when oxygen was added to the highly reactive and strongly nonthermal laser plasma generated in a laser ablation cluster source.[23] Here we find the gold cations Au_x^+ ($x \geq 2$) to be nonreactive toward molecular oxygen under thermal reaction conditions, in agreement with earlier investigations under comparable conditions.[17,24−26]

For molecular hydrogen the dependence of the reactivity on the gold cluster charge state is reversed, with the anionic clusters Au_x^- found to be nonreactive.[17] In contrast, the adsorption of H_2 on Au_x^+ has been observed under multicollision conditions in a flow-tube reactor experiment,[17,26] while the process does not occur under single-collision conditions at room temperature.[27]

In this paper we present experiments and first-principles density-functional theory (DFT) calculations on gas-phase reactions of small gold clusters, aiming at elucidation of the role of hydrogen in the activation of molecular oxygen. Positively charged gold clusters Au_x^+ ($x = 2-7$) were chosen because electronic factors and experimental data suggest them to be most suitable for promoting the oxidation of unsaturated hydrocarbons.[28] Our investigations show that, although small gas-phase gold cluster cations are known to be inert toward molecular oxygen,[17,25] the preadsorption of molecular hydrogen cooperatively enables the adsorption of O_2 on the even-size Au_x^+ clusters. Moreover, investigations of the temperature- and reaction-time-dependent ion intensities, occurring in an octopole ion trap under multicollision conditions,[29] indicate that hydrogen promotes the activation of molecular oxygen on Au_4^+ and Au_6^+, culminating in the dissociation of O_2 at temperatures as low as 200 K. The detailed mechanisms of hydrogen-induced oxygen activation, involving formation of a hydroperoxo transition complex and the elimination and desorption of H_2O, are revealed with the use of DFT calculations.

The paper is organized as follows. In section 2 we describe the experimental setup, data evaluation procedure, and theoretical methods. Our results are presented in section 3, with the experimental findings described first in section 3.1. The theoreti-

(10) Bernhardt, T. M.; Heiz, U.; Landman, U. In *Nanocatalysis*; Heiz, U., Landman, U., Eds.; Springer-Verlag: Berlin, 2007.
(11) (a) Ricci, D.; Bongiorno, A.; Pacchioni, G.; Landman, U. *Phys. Rev. Lett.* **2006**, *97*, 036106. (b) Zhang, C.; Yoon, B.; Landman, U. *J. Am. Chem. Soc.* **2007**, *129*, 2228.
(12) Yoon, B.; Häkkinen, H.; Landman, U.; Wörz, A. S.; Antonietti, J.-M.; Abbet, S.; Judai, K.; Heiz, U. *Science* **2005**, *307*, 403.
(13) Socaciu, L. D.; Hagen, J.; Bernhardt, T. M.; Wöste, L.; Heiz, U.; Häkkinen, H.; Landman, U. *J. Am. Chem. Soc.* **2003**, *125*, 10437.
(14) Hayashi, T.; Tanaka, K.; Haruta, M. *J. Catal.* **1998**, *178*, 566.
(15) Varganov, S. A.; Olson, R. M.; Gordon, M. S.; Mills, G.; Metiu, H. *J. Chem. Phys.* **2004**, *120*, 5169.
(16) Min, B. K.; Friend, C. M. *Chem. Rev.* **2007**, *107*, 2709.
(17) Cox, D. M.; Brickman, R.; Creegan, K.; Kaldor, A. *Z. Phys. D* **1991**, *19*, 353.
(18) Salisbury, B. E.; Wallace, W. T.; Whetten, R. L. *Chem. Phys.* **2000**, *262*, 131.
(19) (a) Bernhardt, T. M.; Socaciu-Siebert, L. D.; Hagen, J.; Wöste, L. *Appl. Catal., A* **2005**, *291*, 170. (b) Lee, T. H.; Ervin, K. M. *J. Phys. Chem.* **1994**, *98*, 10023. (c) Stolcic, D.; Fischer, M.; Ganteför, G.; Kim, Y. D.; Sun, Q.; Jena, P. *J. Am. Chem. Soc.* **2003**, *125*, 2848.
(20) Yoon, B.; Häkkinen, H.; Landman, U. *J. Phys. Chem. A* **2003**, *107*, 4066.
(21) Yoon, B.; Koskinen, P.; Huber, B.; Kostko, O.; von Issendorf, B.; Häkkinen, H.; Moseler, M.; Landman, U. *ChemPhysChem* **2007**, *8*, 157.
(22) (a) Ding, X.; Li, Z.; Yang, J.; Hou, J. G.; Zhu, Q. *J. Chem. Phys.* **2004**, *120*, 9594. (b) Torres, M. B.; Fernández, E. M.; Balbás, L. C. *J. Phys. Chem. A* **2008**, *112*, 6678.
(23) (a) Bürgel, C.; Reilly, N. M.; Johnson, G. E.; Mitrić, R.; Kimble, M. L.; Castleman, A. W., Jr.; Bonačeić-Koutecký, V. *J. Am. Chem. Soc.* **2008**, *130*, 1694. (b) Johnson, G. E.; Reilly, N. M.; Tyo, E. C.; Castleman, A. W., Jr. *J. Phys. Chem. C* **2008**, *112*, 9730. (c) Kimble, M. L.; Castleman, J., A. W. *Int. J. Mass Spectrom.* **2004**, *233*, 99.
(24) Koyanagi, G. K.; Caraiman, D.; Blagojevic, V.; Bohme, D. K. *J. Phys. Chem. A* **2002**, *106*, 4581.
(25) Koszinowski, K.; Schröder, D.; Schwarz, H. *ChemPhysChem* **2003**, *4*, 1233.
(26) Cox, D. M.; Brickman, R. O.; Creegan, K.; Kaldor, A. *Mater. Res. Soc. Symp. Proc.* **1991**, *206*, 43.
(27) Sugawara, K.; Sobott, F.; Vakhtin, A. B. *J. Chem. Phys.* **2003**, *118*, 7808.
(28) Chrétien, S.; Gordon, M. S.; Metiu, H. *J. Chem. Phys.* **2004**, *121*, 3756.
(29) Bernhardt, T. M. *Int. J. Mass Spectrom.* **2005**, *243*, 1.

cal results are given in section 3.2, with an analysis of hydrogen and oxygen binding on Au_4^+ and Au_6^+ given in section 3.2.1.1 and section 3.2.1.2, respectively. Reaction pathways proceeding via Langmuir−Hinshelwood or Eley−Rideal mechanisms are displayed and analyzed in section 3.2.2 (with reactions on Au_4^+ discussed in section 3.2.2.1 and reactions on Au_6^+ in section 3.2.2.2); our discussion includes analysis of the formation of transition-state complexes and interaction intermediates leading to the dissociation of O_2. The theoretical results agree well with the experimental findings, and they provide useful insights pertaining to the nature of bonding, activation, and reactions of coadsorbed hydrogen and oxygen on small gold cation clusters. We summarize our results in section 4.

2. Methods

2.1. Experimental Setup. The experimental setup used in the study of the Au_x^+ ($x = 2-7$) cluster reactions consists of a variable-temperature radio frequency (rf) octopole ion trap inserted into a low-energy ion beam assembly of two quadrupole mass spectrometers and two ion guides. Since the general experimental setup is described in detail elsewhere, we limit ourselves here to a brief outline of certain pertinent elements of the experiment.[29,30]

Four high-energy xenon ion beams of a CORDIS (cold reflex discharge ion source)[31] simultaneously sputter four metal targets which release small metal clusters, consisting of neutrals and ions, in the size range of a few atoms. Clusters of the desired charge state are introduced into a helium-filled quadrupole, which serves to collimate and thermalize the hot cluster ions. Subsequently, cluster ions with the desired size are selected from the beam by a mass-selective quadrupole filter and are steered through an ion-guiding quadrupole into the home-built octopole ion trap. The trap is prefilled with helium (at about 1 Pa total pressure) and the reactive gases (H_2 and O_2). The absolute pressure inside the trap is measured by a Baratron gauge (MKS, type 627B, regulation and detection accuracy 0.01 Pa). The ion trap is attached to a helium cryostat that allows for temperature adjustment in the range between 20 and 300 K. Thermal equilibration of the clusters is achieved within a few milliseconds (about 10^3 collisions) under our experimental conditions,[29] while the clusters are stored for a considerably longer time, typically between 0.1 s and several seconds. After the chosen reaction time, i.e., storage time, t_R, all ions, intermediates, and products are extracted by applying a pulsed bias potential to the exit lens of the ion trap. The ion distribution is subsequently analyzed by a second quadrupole mass filter. To account for a slightly asymmetric mass peak shape occurring at very low ion intensities in our apparatus, the raw data have been deconvoluted with a constant apparatus function to yield the shown mass spectra.[32]

To obtain experimental insights into the reaction mechanisms discussed below, we recorded ion mass distributions while changing three pertinent parameters: (i) the cluster size (Au_x^+, $x = 2-7$), (ii) the reaction temperature, T_R (300, 200, and 100 K), and (iii) the reaction time, t_R (0.1−2 s). During all the experiments the total pressure in the ion trap was fixed to about 1.0 Pa (0.97−1.27 Pa), including the reactant partial pressures of 20% oxygen and 10% hydrogen.

2.2. Data Evaluation. To interpret and understand the experimental data, in particular with respect to the temperature dependencies, it is necessary to briefly outline the reaction models underlying the measured processes.[13,29] As an example, the straightforward association reaction

$$Au_x^+ + H_2 \rightarrow Au_xH_2^+ \quad (1)$$

is discussed in the following. Note that the models are exactly the same for the molecular oxygen coadsorption discussed later in this paper.

Since the total pressure inside the ion trap is about 1 Pa, and therefore the experiments are performed in the kinetic low-pressure regime, a Lindemann-type mechanism has to be considered for each reaction step. Furthermore, the concentrations of the reactive gases, as well as the buffer gas in the ion trap, are orders of magnitude larger than the Au_x^+ concentration, and a steady flow of the reactants is ensured. This permits the postulation of pseudo-first-order kinetics for all proposed reaction steps.

The details of reaction 1 are described by the Lindemann energy transfer model for association reactions,[33] which is presented by the following equations:

$$Au_x^+ + H_2 \underset{k_d}{\overset{k_a}{\rightleftarrows}} (Au_xH_2^+)^* \quad (2a)$$

$$(Au_xH_2^+)^* + He \xrightarrow{k_s} Au_xH_2^+ + He^* \quad (2b)$$

The reaction model includes three elementary steps: (1) the formation of an energized complex $(Au_xH_2^+)^*$ (k_a) and (2) the potential unimolecular decomposition back to the reactants (k_d), in competition with (3) a stabilizing energy transfer collision (k_s) with helium buffer gas or also with other reactant molecules (omitted in eq 2b for the sake of clarity). The ion−molecule association rate constant, k_a, and the final stabilization rate constant, k_s, are well represented by ion−molecule collision rate coefficients as specified by the Langevin theory.[33,34] According to this theory, ion−molecule reactions are basically interactions between a charge and an induced dipole and thus exhibit no activation barrier and hence no temperature dependence of the rate coefficients. Therefore, any observed temperature dependence must be contained in the unimolecular decomposition rate constant, k_d. The activation barrier of this unimolecular decomposition results in a negative temperature dependence for the overall reaction (eq 1). This means, vice versa, that whenever a negative temperature dependence is observed in the experiments, a barrier-free reaction pathway can be assumed. In contrast, a positive temperature dependence would indicate an activated reaction mechanism.

2.3. Computational Methods. In explorations of the atomic arrangements and electronic structures of gold cluster cations, the binding characteristics and structures of molecules adsorbing on such clusters, and the mechanisms of reactions catalyzed by these clusters, we have used first-principles DFT calculations. In particular, we employed the Born−Oppenheimer (BO) spin density functional (SDF) molecular dynamics (MD) method, BO-SDF-MD,[35] with norm-conserving soft pseudopotentials (including a scalar relativistic pseudopotential for Au)[36] and the generalized gradient approximation (GGA)[37] for electronic exchange and correlations. In these calculations we have used a plane wave basis with a kinetic energy cutoff of 62 Ry. The BO-SDF-MD method[35] is particularly suitable for investigations of charged systems since it does not employ a supercell (i.e., no periodic replication of the ionic system is used). Structural optimizations were performed using a conjugate-gradient-like method. Previous investigations of gold clusters (as well as other clusters) and their chemical reactivity using the above methodology have yielded results in good agreement with

(30) Socaciu, L. D.; Hagen, J.; Heiz, U.; Bernhardt, T. M.; Leisner, T.; Wöste, L. *Chem. Phys. Lett.* **2001**, *340*, 282.
(31) Keller, R.; Nöhmeier, F.; Spädtke, P.; Schönenberg, M. H. *Vacuum* **1984**, *34*, 31.
(32) Lang, S. M.; Bernhardt, T. M. *Eur. Phys. J. D* **2009**, *52*, 139.
(33) Steinfeld, J. I.; Francisco, J. S.; Hase, W. L. *Chemical Kinetics and Dynamics*, 2nd ed.; Prentice Hall: Upper Saddle River, NJ, 1999.
(34) Langevin, P. M. *Ann. Chem. Phys.* **1905**, *5*, 245.
(35) Barnett, R. N.; Landman, U. *Phys. Rev. B* **1993**, *48*, 2081.
(36) Troullier, N.; Martins, J. L. *Phys. Rev. B* **1991**, *43*, 1993.
(37) Perdew, J. P.; Burke, K.; Ernzerhof, M. *Phys. Rev. Lett.* **1996**, *77*, 3865.

experimental findings. We remark here that such calculations have been shown to give very accurate bond lengths (up to 1% too long) and reaction barriers that are accurate to within 25%−30% (usually too low; see p 87 of ref 4).

For each of the cluster systems that we consider in this study we explored several reaction mechanisms corresponding to the various model catalyst systems investigated in the experiments. The reaction profiles (pathways) that we present were obtained via first-principles quantum calculations described above. In these calculations a reaction coordinate was judiciously chosen; the reaction coordinate may consist of several geometrical parameters pertinent for the studied mechanism; for example, a reaction coordinate may entail at a certain stage of the reaction the distance between two reacting atoms, e.g., the distance between an O atom of an adsorbed oxygen molecule and the nearest H atom of a coadsorbed hydrogen molecule, while at a subsequent stage the pertinent reaction coordinate may correspond to the rotation angle of a chosen molecular group. For each value of the reaction coordinate, the total energy of the system was optimized through unconstrained relaxation of all of the other degrees of freedom of the system (reactant molecules and gold cluster atoms). The reaction profiles were obtained via repeating such calculations for various values of the chosen reaction coordinate; we note that no distance (or angle) scales are attached to the horizontal axes of the reaction profiles (see Figures 11−14). These calculations yield results that are the same as, or close to, those obtained by other methods (e.g., the nudged elastic band and variants thereof; see the discussion on pp 89 and 90 in ref 4).

3. Results

3.1. Experimental Results. In the first set of experiments we investigated the reaction of Au_x^+ ($x = 2-7$) toward pure hydrogen and oxygen independently. As already mentioned in the Introduction, in complete agreement with previous studies under thermal conditions,[17,25,26] small gold cluster cations are found to be entirely unreactive toward molecular oxygen at any temperature investigated. In contrast, a distinct temperature- and cluster-size-dependent reaction behavior toward molecular hydrogen is observed.

3.1.1. H_2 Adsorption. Only products of the stoichiometry $Au_xH_y^+$ ($y = 2, 4, ..., 12$) are detected. Although it cannot be determined on the basis of our experimental results alone whether hydrogen retains its molecular structure, coordinates to the cluster with both hydrogen atoms,[38] or even dissociates on the cluster as previously predicted theoretically,[15] coadsorption experiments with nitrogen indicate that H_2 is adsorbed molecularly, because N_2 and H_2 are found to compete for the same adsorption sites and reactant partial-pressure-dependent adsorbate exchange is observed.

At a reaction temperature of $T_R = 300$ K none of the investigated clusters form any stable reaction products with molecular hydrogen, except Au_5^+, which adsorbs up to three H_2 molecules at a reaction time $t_R = 0.5$ s. Cooling to 200 K changes the reaction behavior dramatically. While the gold dimer is still unreactive, Au_3^+ and Au_4^+ adsorb up to three, Au_5^+ and Au_6^+ up to four, and Au_7^+ up to two hydrogen molecules. At this temperature the reactions of Au_4^+, Au_5^+, and Au_7^+ are already so fast that even at the shortest measured reaction time ($t_R = 0.1$ s) no pure metal cluster signal can be observed. Further lowering the temperature to 100 K leads to an almost instantaneous size-dependent hydrogen saturation of the clusters. Figure 1 shows the maximum (saturation) number of adsorbed hydrogen molecules at $T_R = 100$ K.

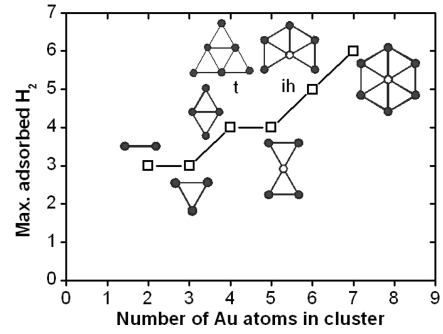

Figure 1. Cluster-size-dependent hydrogen saturation at $T_R = 100$ K and minimum-energy structures of the investigated cluster sizes[41] (see also Figures 6 and 8−10). "Corner" site atoms are indicated by filled circles. For the case of Au_6^+ the two lowest energy isomers are displayed with the nontriangular incomplete hexagonal (ih) isomer being 0.19 eV higher in energy than the triangular (t) one (see Figure 9).

Up to the gold pentamer these cluster-size-dependent hydrogen saturation levels are in perfect agreement with previous experiments by Cox et al.;[17,26] in the earlier experiment saturation was not reached only for $x = 6$ and 7. We note that our observed correlation between the H_2 saturation numbers and the number of "corner" atoms in the clusters (see the discussion below) agrees with earlier findings obtained from saturation measurements for $Au^{32}{}_x^+$ with CO,[39] methane (CH_4)[32,40] and ethylene (C_2H_4)[40] as long as the gold clusters do not experience adsorbate induced structural changes.[39]

To analyze possible binding sites, we also display the reported[41] (see also Figures 6 and 8−10) minimum-energy structures of Au_x^+ in Figure 1. Generally, H_2 acts as an electron-density-donating ligand to transition-metal cations,[42] and consequently, the binding of hydrogen to a particular site of the gold cluster cation is expected to correlate with the localization of the cluster lowest unoccupied molecular orbital (LUMO).[43] Recent DFT calculations indicate that the LUMO of the bare cluster is primarily located on corner atoms, where it protrudes most into the vacuum.[28] As a result, hydrogen will preferably bind to corner atoms, whereas no adsorption on central atoms or cluster flat faces is expected.[28] Indeed, the results of our measurements (as well as our DFT calculations for Au_4^+ and Au_6^+; see below) show for all the Au_x^+ clusters, except Au_2^+, saturation numbers of adsorbed hydrogen molecules that equal the number of gold atoms positioned at corner sites in the corresponding ground-state (lowest energy) geometries (cf. Figure 1; see also Figures 6 and 8−10). Only in the case of Au_6^+ the maximum number of H_2 molecules agrees better with the higher energy isomeric structure (the nontriangular, incomplete hexagonal (ih) geometry displayed in Figure 1). Indeed, our DFT calculations show that the Au_6^+ cluster undergoes, upon hydrogen adsorption, isomerization from a triangular ground-state geometry of the bare cluster to the nontriangular, incomplete hexagonal, geometry (see Figures 9 and 10).

(38) Ghebriel, H. W.; Kshirsagar, A. *J. Chem. Phys.* **2007**, *126*, 244705.
(39) Fielicke, A.; von Helden, G.; Meijer, G.; Pedersen, D. B.; Simard, B.; Rayner, D. M. *J. Am. Chem. Soc.* **2005**, *127*, 8416.
(40) Buratto, S. K.; Bowers, M. T.; Metiu, H.; Manard, M. J.; Tong, X.; Benz, L.; Kemper, P.; Chrétien, S. In *Atomic Clusters: From Gas Phase to Deposited*; Woodruff, D. P., Ed.; Elsevier: Amsterdam, 2007; Vol. 12, p 151.
(41) Gilb, S.; Weis, P.; Furche, F.; Ahlrichs, R.; Kappes, M. M. *J. Chem. Phys.* **2002**, *116*, 4094.
(42) Kubas, G. J. *Chem. Rev.* **2007**, *107*, 4152.
(43) Manard, M. J.; Kemper, P. R.; Bowers, M. T. *J. Am. Chem. Soc.* **2005**, *127*, 9994.

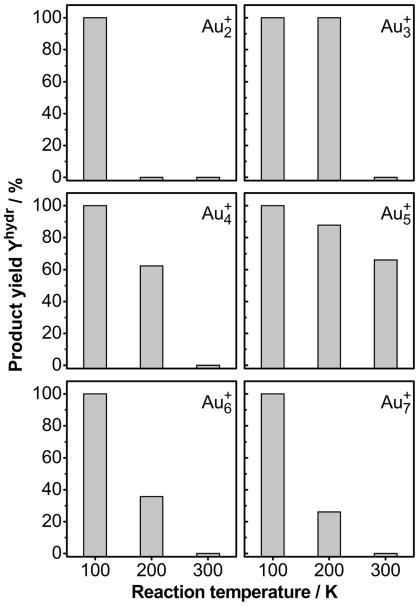

Figure 2. Bar charts of the hydrogen adsorption on Au_x^+ after the cluster ions were trapped for $t_R = 0.5$ s as a function of temperature. The height of the bars represents the ratio of the hydrogen coverage to the maximum hydrogen adsorption as defined by eq 3.

To further illustrate the temperature dependence of the hydrogen adsorption to the gold cluster cations, we display in Figure 2 the hydrogen adsorption on Au_x^+ at a fixed reaction time $t_R = 0.5$ s. Since for this representation one should consider in addition to the temperature dependence of the reaction rate (and thus the extent of reaction at a given temperature) the amount of adsorbed hydrogen molecules, the height of the bars Y^{hydr} reflects, for each cluster size, the ratio of the actual hydrogen coverage to the maximum (saturation) hydrogen coverage, calculated by

$$Y^{hydr} = \frac{\sum_{i=0}^{y_{max}} \frac{I_i}{I_{prod}} i}{y_{max}} \times 100\% \qquad (3)$$

where I_i denotes the intensity of the product peak corresponding to i adsorbed hydrogen atoms, I_{prod} is the sum of the intensities of all products, and y_{max} denotes the saturation number of adsorbed hydrogen atoms. From the bar charts in Figure 2 it is apparent that for all cluster sizes hydrogen adsorption is accelerated by decreasing the reaction temperature. This negative temperature dependence indicates a barrier-free hydrogen adsorption, as discussed in section 2.

3.1.2. Coadsorption of O_2 and H_2. Next, at a reaction temperature of $T_R = 100$ K a mixture of the reactive gases H_2 and O_2 was introduced into the ion trap at a ratio of 1:2. Figure 3 displays ion mass distributions obtained after the Au_x^+ clusters were trapped at 100 K for $t_R = 0.1$ s; the labels (x,y,z) next to the mass spectral peaks correspond to the number of gold atoms in the cluster cation (x) and the numbers of adsorbed hydrogen (y) and oxygen (z) atoms. A striking odd−even alternation is observed in the mass spectra: while all the odd cluster sizes ($x = 3$, 5, and 7) reach almost instantaneously their hydrogen saturation level as in the case of pure hydrogen exposure (see Figure 1), with no measurable coadsorption of oxygen, the even-size clusters ($x = 2$, 4, and 6) do not achieve complete hydrogen

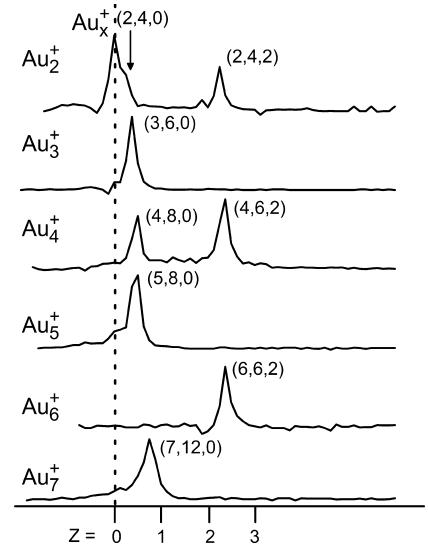

Figure 3. Ion mass distributions for all investigated cluster sizes after Au_x^+ was trapped at $T_R = 100$ K for $t_R = 0.1$ s inside the octopole ion trap filled with helium buffer gas, as well as O_2 and H_2 at a ratio of 2:1. The mass peaks are denoted with (x,y,z) corresponding to complexes of the stoichiometry $Au_xH_yO_z^+$.

saturation and exhibit instead cooperative coadsorption[10,44] of one oxygen molecule ($z = 2$) in addition to hydrogen. The coadsorption of multiple O_2 molecules has not been observed even at higher O_2 pressures and extended reaction times.

As molecular oxygen does not react with Au_x^+, hydrogen preadsorption is responsible for the activation of the gold clusters to enable cooperative oxygen coadsorption. Cooperative coadsorption is known to be an important reactivity-promoting process for small metal clusters and nanoparticles.[13,44]

In a simple valence electron structure model the odd−even alternation in the O_2 coadsorption can be attributed to the fact that odd-size gold cluster cations exhibit a closed-shell valence electron structure leading to a low binding energy for the hydrogen-promoted oxygen adsorption.[18,20,29,45] In contrast, even-size gold cluster cations possess an unpaired valence electron that, upon hydrogen activation, may interact with the two unpaired electrons occupying the $2\pi_g^*$ antibonding orbital of the oxygen molecule, resulting in stable complexes; the mechanism of reaction between charged gold clusters and O_2, involving the antibonding molecular orbitals of the oxygen molecule, has been elucidated for the case of gold anions, Au_x^-, where (in the context of the oxidation of CO) it has been shown that this bonding mechanism serves to weaken (i.e., activate) the O−O bond of the adsorbed oxygen molecule.[2,5,9,10,12] The use of this picture for explaining the mechanism of the observed promotion of the reactivity of the cluster cations toward O_2, occurring through the preadsorption (or coadsorption) of hydrogen, will be addressed below when we discuss our theoretical calculations.

We focused in the experiments, as well as in the theoretical investigations, on the even-size cluster ions Au_4^+ and Au_6^+, because these clusters are the only investigated clusters that exhibit hydrogen-induced oxygen coadsorption at temperatures

(44) Lang, S.; Popolan, D. M.; Bernhardt, T. M. In *Atomic Clusters: From Gas Phase to Deposited*; Woodruff, P., Ed.; Elsevier: Amsterdam, 2007; Vol. 12, p 53.
(45) Varganov, S. A.; Olson, R. M.; Gordon, M. S.; Metiu, H. *J. Chem. Phys.* **2003**, *119*, 2531.

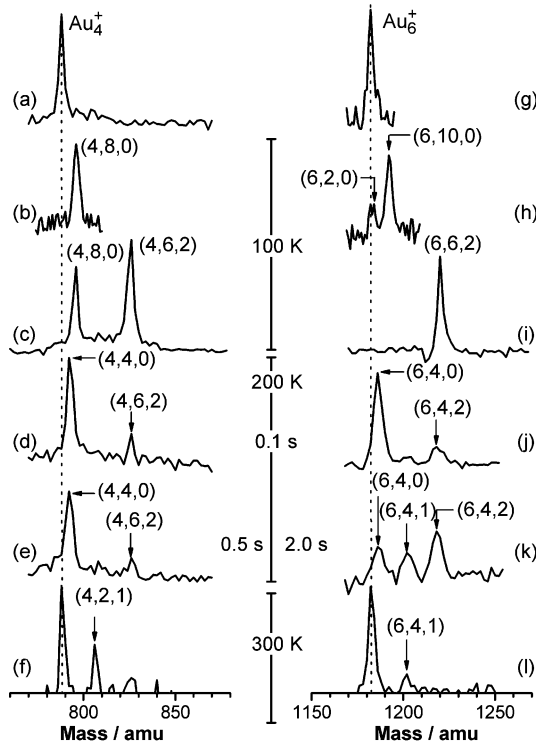

Figure 4. Sequences of mass spectra of the ion trap content illustrating the temperature- and reaction-time (storage-time)-dependent activation of molecular oxygen by Au_4^+ (a−f) and Au_6^+ (g−l). Traces a and g were obtained in the absence of any reactive gases, traces b and h in the presence of pure hydrogen ($t_R = 0.1$ s), and traces c−f and i−l in the presence of both molecular hydrogen and oxygen ($t_R = 0.1$ s in (c), (d), (i), and (j); $t_R = 0.5$ s in (e) and (l); $t_R = 2$ s in (k) and (f); no changes in the product distributions are observed at longer reaction times). The mass peaks are denoted with (x,y,z) corresponding to $Au_xH_yO_z^+$.

above 200 K, which eventually leads to the dissociation of O_2 on the clusters. Further experimental information can be gained from temperature- and reaction-time-dependent measurements.

Representative product mass spectra of Au_4^+ and Au_6^+ obtained under various reaction conditions are assembled in Figure 4; the data in the left (a−f) (right (g−l)) column correspond to the Au_4^+ (Au_6^+) cluster, respectively. The topmost traces (a, g) show the pure mass signals of the metal cluster in the absence of any reactive gases. Mass spectra obtained after the addition of hydrogen at a reaction temperature of 100 K are depicted in the second topmost traces (b, h). As detailed above, and in agreement with previous experiments, under multicollision conditions[17] H_2 is found to adsorb on Au_x^+ clusters, leading to the maximum coverage species $Au_4H_8^+$ (mass peak in (b) labeled (4,8,0)) and $Au_6H_{10}^+$ (mass peak in (h) labeled (6,10,0)); the corresponding saturated coverage calculated configurations ($Au_4H_8^+$ and $Au_6H_{10}^+$), with one H_2 molecule attached to each of the undercoordinated corner Au atoms, are shown in Figures 6a, 8a, and 10a, with the average binding energies per H_2 molecule being 0.53 and 0.38 eV for Au_4^+ and Au_6^+, respectively.

Adding both H_2 and O_2 to the ion trap at 100 K yields the coadsorption products $Au_4H_6O_2^+$ and $Au_6H_6O_2^+$ even at a very short reaction time $t_R = 0.1$ s (Figure 4; see the mass peak labeled (4,6,2) in trace (c) and the one labeled (6,6,2) in trace (i); cf. also Figure 3). When the reaction time is kept constant at 0.1 s, but the ion trap is heated to 200 K, the signal intensity of the coadsorption product $Au_4H_6O_2^+$ decreases (Figure 4, trace d). In addition, under these conditions, $Au_4H_4^+$ is detected

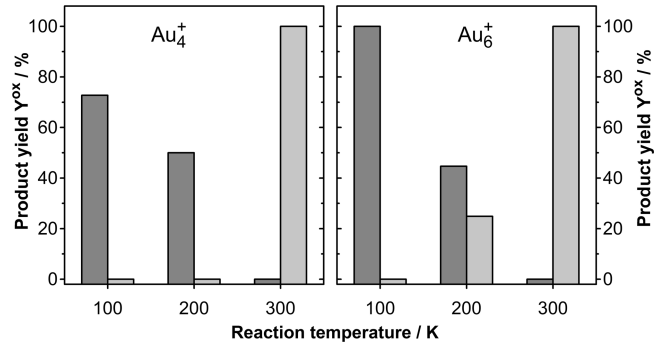

Figure 5. Bar charts of the temperature dependence of oxygen adsorption on Au_4^+ and Au_6^+ ($Au_xH_yO^+$, light gray bars; $Au_xH_yO_2^+$, dark gray bars). The heights of the bars for $Au_xH_yO^+$ and $Au_xH_yO_2^+$ correspond to the relative intensities of the peaks in the ion mass spectra (eq 4) at a reaction time of $t_R = 2$ s.

instead of $Au_4H_8^+$. Increasing the reaction time to 0.5 s does not notably change the intensity of these products (trace e). Also no additional products are observed at longer reaction times. A further increase in temperature to 300 K, however, alters the product mass spectrum drastically. From trace f it is apparent that no hydrogen adsorption products are observed anymore; instead the bare Au_4^+ signal reappears together with a new mass peak corresponding to the mass of $Au_4H_2O^+$ containing a single oxygen atom. In contrast, the $Au_4H_6O_2^+$ peak decreases in relative intensity, reflecting the dissociation of the initially coadsorbed O_2 molecule.

The activation and dissociation of the coadsorbed oxygen molecule with increasing temperature is even more apparent for Au_6^+. In this case, the coadsorption product $Au_6H_6O_2^+$ is the sole mass signal at 100 K, when O_2 and H_2 are admitted to the trap (Figure 4, trace i). At the same reaction time of 0.1 s, but at 200 K, $Au_6H_4O_2^+$ is detected in addition to $Au_6H_6O_2^+$ as well as $Au_6H_4^+$ (trace j). Trace k in Figure 4, obtained at an increased reaction time of 2.0 s and 200 K, reveals that $Au_6H_4^+$, $Au_6H_4O_2^+$, and $Au_6H_6O_2^+$ are still apparent while an additional mass peak corresponding to $Au_6H_4O^+$ emerges. Hence, in the case of Au_6^+ the dissociation of the coadsorbed O_2 already proceeds at 200 K. Further heating the ion trap to 300 K causes both $Au_6H_4^+$ and the coadsorption products $Au_6H_4O_2^+$/ $Au_6H_6O_2^+$ to vanish. Only $Au_6H_4O^+$, containing a single oxygen atom, is detected (trace l) along with the unreacted bare Au_6^+ cluster.

The temperature dependence of the $Au_6H_yO_2^+$ and $Au_6H_yO^+$ product formation is further detailed in Figure 5 in a bar graph representation and shows the same behavior as in the case of Au_4^+. The intensity of the product signal, I, corresponding to products of the stoichiometries $Au_xH_yO^+$ (light gray bars) and $Au_xH_yO_2^+$ (dark gray bars) relative to the intensity of all products, I_{prod} (excluding the pure metal cluster peak), is calculated and plotted as the reaction yield, Y^{Ox}

$$Y^{Ox} = \frac{I}{I_{prod}} \times 100\% \qquad (4)$$

as a function of the reaction temperature. Note that at a given temperature the sum of the heights of the light and dark gray bars may not necessarily reach 100%, since the adsorption of hydrogen by the cluster, which increases the total product intensity, is not necessarily accompanied by oxygen coadsorption.

From Figure 5 we observe that for both Au_4^+ and Au_6^+ clusters the reaction yield, Y^{Ox}, of $Au_xH_yO_2^+$ products (dark gray

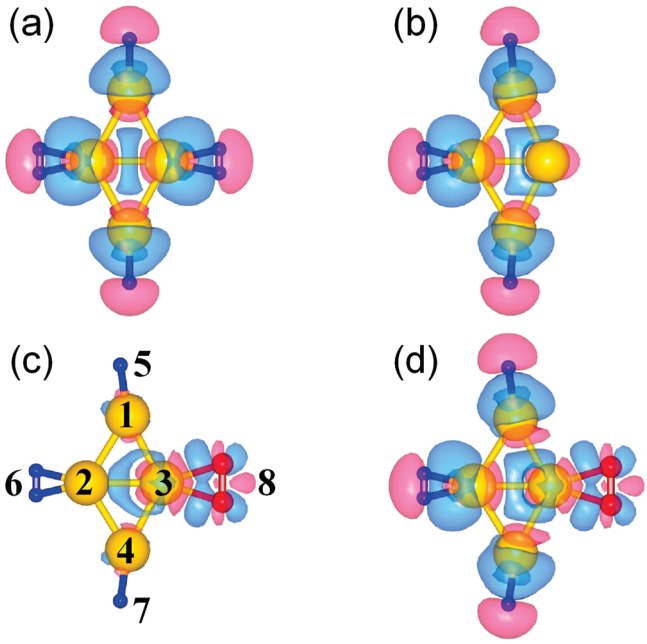

Figure 6. Difference charge density isosurfaces (encompassing 90% of the charge) for (a) the saturation coverage cluster $Au_4(H_2)_4^+$, (b) $Au_4(H_2)_3(3c,2c,2c)^+$, and (c, d) $Au_4(H_2)_3(3c,2c,2c)O_2(3c)^+$. The charge density differences are calculated as (a) $\rho_{tot} - \rho[Au_4^+] - \rho[4H_2]$, (b) $\rho_{tot} - \rho[Au_4^+] - \rho[3H_2]$, (c) $\rho_{tot} - \rho[Au_4(H_2)_3^+] - \rho[O_2]$, and (d) $\rho_{tot} - \rho[Au_4^+] - \rho[3H_2] - \rho[O_2]$; ρ_{tot} is the total charge density of the gold cluster cation with the adsorbed molecules. Blue regions correspond to excess electronic charge, and pink ones correspond to charge deficiency. Note that charge difference plot c pertains to the effect of coadsorption of O_2 onto the $Au_4(H_2)_3^+$ cluster (see (b)), while charge difference plot d pertains to the effect of the adsorption of both H_2 and O_2 onto the bare Au_4^+ cluster. The difference charge densities are superimposed on the atomic structures, with Au atoms depicted by yellow balls, hydrogen atoms by blue balls, and oxygen atoms by red balls. The numbering scheme of the atoms is displayed in (c). All the cases shown correspond to molecular (nondissociative) adsorption.

bars) shows a negative temperature dependence (that is, the yield decreases with increasing temperature), while for the oxygen dissociation products, $Au_xH_yO^+$, a positive temperature dependence is found. According to Langevin theory and the Lindemann energy transfer model (cf. section 2.2), the negative temperature dependence for $Au_xH_yO_2^+$ can be associated with a barrier-free O_2 adsorption on the cluster. In contrast, the positive temperature dependence for $Au_xH_yO^+$ indicates an activation barrier for the dissociation of O_2. As we discuss below, these assertions are corroborated by our first-principles simulations of the reaction profiles.

3.2. Theoretical Results. In this section we describe our findings obtained through first-principles DFT calculations, pertaining to the geometric arrangements of atoms in bare Au_4^+ and Au_6^+ clusters, the binding characteristics of hydrogen and oxygen molecules to these clusters, and the reaction pathways between the reactant molecules resulting in the formation of species with the compositions observed in the experiments described in the previous section.

3.2.1. Hydrogen and Oxygen Adsorption.

3.2.1.1. Au_4^+ Cluster. The ground-state (lowest energy) structure of the Au_4^+ cluster is a rhombus, with an edge distance $d_{edge}(Au-Au) = 2.68$ Å between neighboring atoms (e.g., the atoms labeled 1 and 2 in Figure 6), and the internal distance between the two closest atoms (the two 3-fold-coordinated atoms, labeled 2 and 3 in Figure 6) being $d_i(Au-Au) = 2.74$ Å; the ground-state geometry of the parent neutral Au_4 cluster is quite similar ($d_{edge}(Au-Au) = 2.70$ Å and $d_i(Au-Au) = 2.64$ Å), with a calculated vertical ionization potential vIP = 7.94 eV and an adiabatic ionization potential aIP = 7.90 eV.

Table 1. Total, $E_b(nH_2)$,and per Molecule, $E_b(nH_2)/n$, Binding Energies of nH_2 Molecules to the Au_4^+ Cluster for Different Adsorption Sites (ads site)[a]

n	$E_b(nH_2)$ (eV)	$E_b(nH_2)/n$ (eV)	ads site
1	0.502	0.502	2c
1	0.621	0.621	3c
2	1.182	0.591	2c,3c
2	1.087	0.543	3c,3c
2	0.847	0.423	2c,2c
3	1.605	0.535	2c,2c,3c
3	1.665	0.555	3c,3c,2c
4	2.128	0.532	3c,3c,2c,2c

[a] 2c and 3c denote, respectively, 2-fold- and 3-fold-coordinated Au atoms in the gold tetramer cation. The adsorption energy of the nth H_2 molecule can be calculated from $\Delta E(H_2; n) = E_b(nH_2) - E_b((n-1)H_2)$. Energies are given in electron volts.

Hydrogen molecules bind nondissociatively to the tetramer cluster cation in an on-top geometry; see Figure 6a corresponding to saturation coverage, with each of the adsorbed hydrogen molecules attached to a gold atom that is equidistant from the two hydrogen atoms of the adsorbed H_2 molecule, $d(Au-H(1)) = 1.88$ Å and $d(Au-H(2)) = 1.88$ Å. At saturation (see Figure 6a), two of the molecules are in the plane ($d(H-H) = 0.82$ Å) of the cluster and the other two ($d(H-H) = 0.815$ Å) are normal to it; the Au−Au distances at H_2 saturation are $d(Au(1)-Au(2)) = 2.75$ Å and $d(Au(2)-Au(3)) = 2.62$ Å. As seen from Table 1, the adsorption energy depends on the number of adsorbed molecules and on the adsorption sites. For example, adsorption of a single H_2 molecule on a 2-fold-coordinated (2c) Au atom (e.g., atoms 1 and 4 in Figure 6c) occurs with an energy $E_b(1H_2; 2c) = 0.50$ eV, while for adsorption at a 3-fold-coordinated (3c) gold atom (e.g., atoms 2 and 3 in Figure 6c) the binding energy is higher, $E_b(1H_2; 3c) = 0.62$ eV. At saturation ($4H_2$) the average binding energy per molecule is 0.53 eV, and the adsorption energy of the fourth H_2 molecule depends on the adsorption sites of the previously adsorbed three H_2 molecules: $\Delta E_b(H_2; 4) = 0.46$ eV if the previous three occupied the (3c,3c,2c) sites, and $\Delta E_b(H_2; 4) = 0.52$ eV when the previous three H_2 occupied the (2c,2c,3c) sites (see Table 1). Binding of molecular hydrogen to the cluster involves charge donation to the gold atoms, estimated for the saturation case (see the charge density difference plots in Figure 6a, with blue corresponding to excess charge) to be 0.15e (distributed equally on the gold atoms).

The binding of an oxygen molecule to the Au_4^+ cluster is also nondissociative, although as we discuss below the molecule may dissociate in a process involving energy barriers (as observed experimentally; see Figure 4). The binding of the O_2 molecule to the cluster is barrierless (as deduced also from the experiments), it is promoted by coadsorption of molecular hydrogen, and it depends on the adsorption site. We focus here on the only case of molecular oxygen adsorption found experimentally, that is, in stoichiometrical notation $Au_4H_6O_2^+$ (labeled (4,6,2) in Figures 3 and 4) and corresponds to the complex $Au_4(H_2)_3O_2^+$. We distinguish two adsorption configurations, where the O_2 molecule binds to a 3-fold- and a 2-fold-coordinated Au atom. In the first one (Figure 6c) the O_2 molecule is bonded to a 3-fold-coordinated Au atom, while of the bonding sites of the three coadsorbed H_2 molecules one is a 3-fold-coordinated Au atom and two are 2-fold-coordinated atoms; i.e., the coadsorption complex may be described as

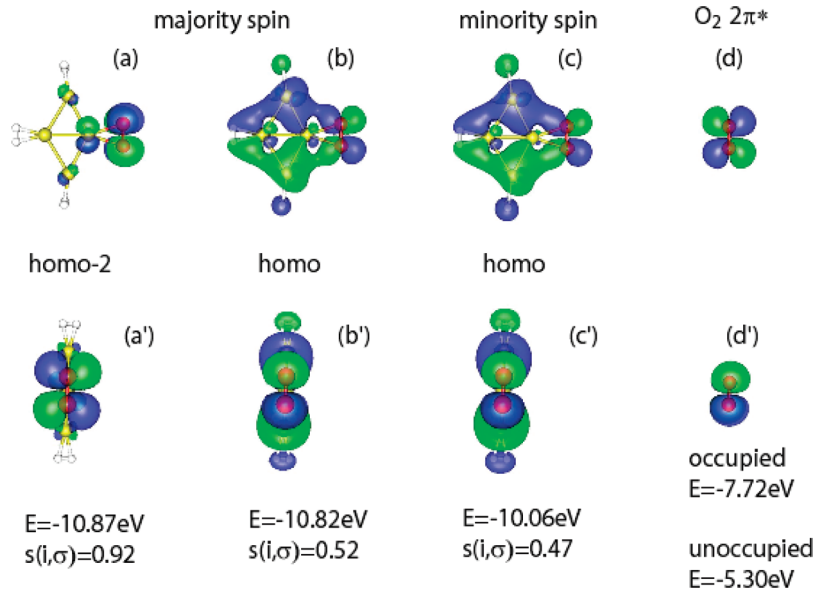

Figure 7. (a−c, a′−c′) Calculated isosurfaces (containing 90% of the norm of the wave function) of the KS orbitals of the $Au_4(H_2)_3(3c,2c,2c)O_2(3c)^+$ cluster which make the largest contributions to the $S(2\pi^*)$ estimator. In each case we show two views of the KS orbital (e.g., a and a′), rotated by 90° with respect to each other. For each orbital, its position in the spectrum (i.e., homo and homo − 2) is given, as well as the energy of the orbital (the Fermi energy is at −9.45 eV) and the value of $s(i,\sigma)$ (see eq 5b). (d, d′) $2\pi^*$ (antibonding) KS orbitals of the isolated O_2 molecule, calculated for the geometry of the adsorbed molecule. These majority spin orbitals (each containing a single electron) have a KS energy eigenvalue of −7.772 eV, while the unoccupied, minority spin orbitals have a higher KS energy (−5.530 eV). Blue and green correspond to positive and negative values of the wave function. The orbitals are superimposed on the atomic structure of the $Au_4(H_2)_3(3c,2c,2c)O_2(3c)^+$ cluster. Au atoms are depicted as yellow balls, hydrogen atoms as light blue balls, and oxygen atoms as red balls.

$Au_4(H_2)_3(3c,2c,2c)O_2(3c)^+$. The total binding energy of the adsorbed molecules is 2.36 eV (with reference to the ground state of the bare Au_4^+ cluster), and the binding energy of the O_2 molecule to the cluster with three H_2 molecules preadsorbed to it (i.e., $Au_4(H_2)_3(3c,2c,2c)^+$) is 0.76 eV; d(Au−O) = 2.23 Å. In this binding state there is excess electronic charge on the O_2 molecule (estimated to be about 0.14e; see Figure 6c,d), and the molecule is activated with an increased interatomic distance d(O−O) = 1.33 Å (compared to 1.25 Å in the gas-phase isolated molecule).

Interestingly, in the $Au_4(H_2)_3(3c,2c,2c)^+$ complex we find that the distribution of the excess electronic charge on the Au atoms (see Figure 6b) differs markedly from that found for the saturation coverage case (Figure 6a). In the present case (Figure 6b), the total excess charge on the gold atoms is estimated to be 0.15e, with 0.09e localized on the bare 3-fold-coordinated Au atom (labeled 3), and the rest distributed evenly on the two 2-fold-coordinated Au atoms (labeled 1 and 4); on the fourth, 3-fold-coordinated Au atom (labeled 2, bonded to one of the H_2 molecules), we estimate a slight charge depletion (0.03e). Coadsorption and accompanying activation of the O_2 molecule (which binds to the 3-fold-coordinated atom labeled 3, which, as aforementioned, carries the largest fraction of the excess electronic charge) involves electronic charge donation (0.14e) to the adsorbed oxygen molecule through occupation of the antibonding $2\pi^*$ orbitals of the molecule, as may be seen from the blue-colored π-orbital-shaped excess charge distribution (having a nodal plane passing through the O−O bond) shown in Figure 6c,d. The degree of population of the antibonding orbitals is estimated to be proportional to $S(2\pi^*) = 0.49$. The estimator $S(2\pi^*)$ expresses the projection of the O_2 molecule $2\pi^*$ orbitals onto the manifold of cluster wave functions. It is calculated as the square of the overlap between the $2\pi^*$ Kohn−Sham (KS) orbitals (calculated separately for the isolated molecule positioned in the adsorption (activated) geometry) and all the KS orbitals of the $Au_4(H_2)_3O_2^+$ complex using the formula

$$S(2\pi^*) = \sum_{\sigma} \sum_{i \in \text{cluster}} f(i,\sigma)\, s(i,\sigma) - 2.0 \qquad (5a)$$

where

$$s(i,\sigma) = \sum_{j \in 2\pi^*} |\langle (i,\sigma)_{\text{cluster}} | (j,\sigma)_{O_2} \rangle|^2 \qquad (5b)$$

In the above equations σ is the spin (taking the values up or down), $\langle (i,\sigma)_{\text{cluster}}|$ is the ith KS orbital of the cluster (with coadsorbed H_2 and O_2 molecules), and $f(i,\sigma)$ is the occupation of that orbital. $|(j,\sigma)_{O_2}\rangle$ is a $2\pi^*$ KS orbital of the isolated O_2 molecule, calculated at the geometry of the molecule adsorbed on the gold cluster. We subtract 2.0 from the sum in eq 5a to account for the majority spin occupancy of the $2\pi^*$ orbitals in the isolated oxygen molecule (which equals 2, corresponding to a single electron in each of the two antibonding orbitals, responsible for the paramagnetic character of the isolated molecule); the maximum occupancy of the two antibonding orbitals is 4, with two electrons occupying each of the spin directions. As a result of this subtraction $S(2\pi^*)$ estimates the (excess) minority spin occupation in the adsorbed O_2 molecule.

The calculated cluster KS orbitals which make the largest contribution to the $S(2\pi^*)$ estimator are shown in Figure 7a−c, along with the $2\pi^*$ KS orbitals (each containing a single majority spin electron) of the isolated O_2 molecule (Figure 7d). In each case we denote the position of the orbital in the spectrum (i.e., homo and homo − 2, where "homo" denotes the highest occupied molecular orbital) and give the energy of the orbital (the Fermi energy is at −9.45 eV) and the value of $s(i,\sigma)$ (see

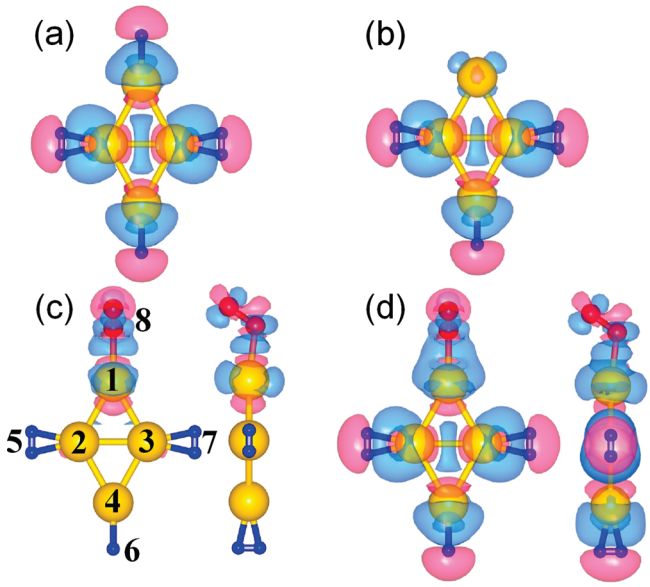

Figure 8. Difference charge density isosurfaces (encompassing 90% of the charge) for (a) the saturation coverage cluster $Au_4(H_2)_4^+$, (b) $Au_4(H_2)_3(3c,3c,2c)^+$, and (c, d) $Au_4(H_2)_3(3c,3c,2c)O_2(2c)^+$. The charge density differences are calculated as (a) $\rho_{tot} - \rho[Au_4^+] - \rho[4H_2]$, (b) $\rho_{tot} - \rho[Au_4^+] - \rho[3H_2]$, (c) $\rho_{tot} - \rho[Au_4(H_2)_3^+] - \rho[O_2]$, and (d) $\rho_{tot} - \rho[Au_4^+] - \rho[3H_2] - \rho[O_2]$; ρ_{tot} is the total charge density of the gold cluster cation with the adsorbed molecules. Blue regions correspond to excess electronic charge, and pink ones correspond to charge deficiency. Note that charge difference plot c pertains to the effect of coadsorption of O_2 onto the $Au_4(H_2)_3^+$ cluster (see (b)), while charge difference plot d pertains to the effect of the adsorption of both H_2 and O_2 onto the bare Au_4^+ cluster. The difference charge densities are superimposed on the atomic structures, with Au atoms depicted by yellow balls, hydrogen atoms by blue balls, and oxygen atoms by red balls; in (c) and (d) we include (on the right) views of the cluster rotated by 90°. The numbering scheme of the atoms is displayed in (c). All the cases shown correspond to molecular (nondissociative) adsorption.

eq 5b). We observe that the orbitals that make the largest contribution to the estimator exhibit an antibonding ($2\pi^*$) character in the vicinity of the adsorbed oxygen molecule (see the right-side region in Figure 7a−c, and compare with Figure 7d); note also the way that this region of the wave function connects to the Au cluster part, showing hybridization of the molecular state with the gold cluster orbitals.

To explore further the promotion effect of hydrogen coadsorption on the binding of an oxygen molecule (and in particular the dependence on the number of coadsorbed H_2 molecules), we consider here O_2 adsorption at a 3-fold-coordinated Au atom (as in Figure 6c discussed above in the context of the maximal number of coadsorbed hydrogen molecules), but, now, in the presence of a single coadsorbed H_2 molecule. We consider two cases: one where the coadsorbed H_2 molecule binds to a 2-fold-coordinated Au atom (as in configuration B shown in Figure 13) and the other where it binds to a 3-fold-coordinated Au atom (not shown). In the first case, i.e., the $Au_4H_2(2c)O_2(3c)^+$ complex, the binding energy of the adsorbed molecules to the gold cluster cation is 1.10 eV, with the adsorption energy of O_2 to the $Au_4H_2(2c)^+$ complex reduced to 0.59 eV compared to the case of three coadsorbed H_2 molecules discussed above (0.76 eV). The adsorption of oxygen is found here to be accompanied by a slightly smaller degree of bond activation (d(O−O) = 1.32 Å and d(Au−O) = 2.23 Å) and a $2\pi^*$ estimator, $S(2\pi^*) = 0.45$. For the case of H_2 coadsorption on the 3c site the binding energy of the adsorbed molecules in the $Au_4H_2(3c)O_2(3c)^+$ complex is 1.05 eV with the adsorption

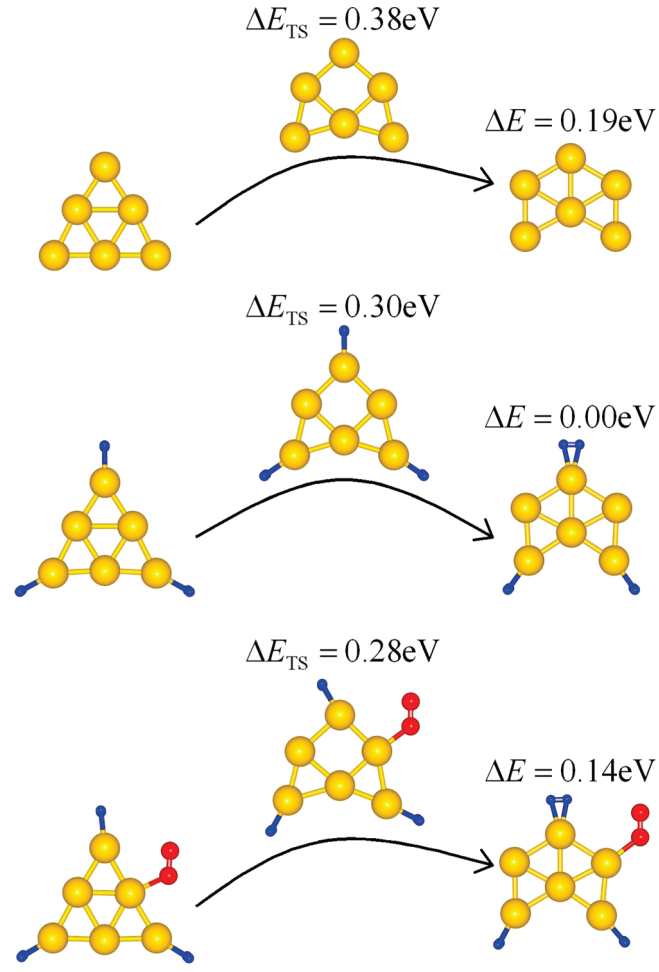

Figure 9. Atomic structures of the gold hexamer cation clusters and transition energies. Top row, bare clusters: left column, triangular ground state $Au_6(t)^+$; middle column, transition state, with $\Delta E_{TS} = 0.38$ eV; right column, incomplete hexagonal isomer $Au_6(ih)^+$. Middle row, $Au_6(H_2)_3^+$ clusters: left column, triangular $Au_6(t)(H_2)_3^+$; middle column, transition state, with $\Delta E_{TS} = 0.30$ eV; right column, incomplete hexagonal isomer $Au_6(ih)(H_2)_3^+$. Bottom row, coadsorption clusters $Au_6(H_2)_3O_2^+$: left column, triangular cluster $Au_6(t)(H_2)_3O_2^+$; middle column, transition state, with $\Delta E_{TS} = 0.28$ eV; right column, incomplete hexagonal $Au_6(ih)(H_2)_3O_2^+$. Au atoms are depicted by yellow balls, hydrogen atoms by blue balls, and oxygen atoms by red balls.

energy of O_2 calculated to be reduced to 0.43 eV. Here we find an additional slight reduction in bond activation (d(O−O) = 1.31 Å) and a corresponding smaller value of the estimator $S(2\pi^*) = 0.36$. For the reaction paths leading to dissociation of the adsorbed oxygen molecule in the presence of preadsorbed hydrogen see our discussion below.

The dependence of the oxygen adsorption characteristics on the adsorption configuration is illustrated through consideration of the $Au_4(H_2)_3(3c,3c,2c)O_2(2c)^+$ complex, shown in Figure 8c,d. Here the oxygen molecule is anchored to a 2-fold-coordinated Au atom (labeled 1 in Figure 8c), with only one of the O atoms bonded directly to the Au atom of the cluster (d(Au−O) = 2.14 Å), and the molecule forms an angle of 120° with respect to the plane of the Au_4^+ cluster (see the side view in Figure 8c). Here the total binding energy of the adsorbed molecules is 2.19 eV (with reference to the ground state of the bare Au_4^+ cluster), and the binding energy of the O_2 molecule to the cluster with three H_2 molecules preadsorbed to it (i.e., $Au_4(H_2)_3(3c,3c,2c)^+$) is reduced to 0.52 eV, compared to oxygen adsorption at the 3-fold-coordinated Au atom discussed above.

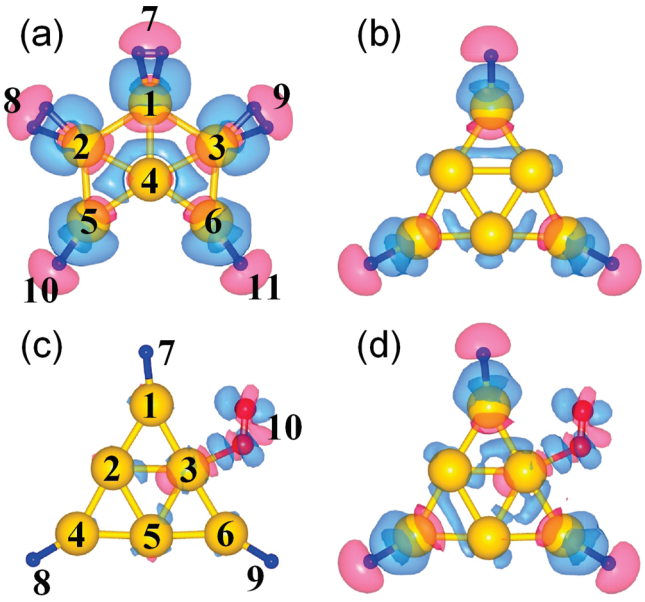

Figure 10. Difference charge density isosurfaces (encompassing 90% of the charge) for (a) the saturation coverage cluster $Au_6(ih)(H_2)_5^+$, (b) $Au_6(t)(H_2)_3^+$, and (c, d) $Au_6(t)(H_2)_3O_2^+$. The charge density differences are calculated as (a) $\rho_{tot} - \rho[Au_6^+] - \rho[5H_2]$, (b) $\rho_{tot} - \rho[Au_6^+] - \rho[3H_2]$, (c) $\rho_{tot} - \rho[Au_6(H_2)_3^+] - \rho[O_2]$, and (d) $\rho_{tot} - \rho[Au_6^+] - \rho[3H_2] - \rho[O_2]$; ρ_{tot} is the total charge density of the gold cluster cation with the adsorbed molecules. Blue regions correspond to excess electronic charge, and pink ones correspond to charge deficiency. Note that charge difference plot c pertains to the effect of coadsorption of O_2 on the $Au_6(H_2)_3^+$ cluster (see (b)), while charge difference plot d pertains to the effect of the adsorption of both H_2 and O_2 onto the bare Au_6^+ cluster. The difference charge densities are superimposed on the atomic structures, with Au atoms depicted by yellow balls, hydrogen atoms by blue balls, and oxygen atoms by red balls. The numbering scheme of the atoms is displayed in (c). All the cases shown correspond to molecular (nondissociative) adsorption.

As in the case discussed above, where for the $(H_2)_3$(3c,2c,2c) configuration of the coadsorbed hydrogen molecules (see Figure 6b) we found that the excess charge (0.15e) in the $Au_4(H_2)_3$(3c,3c,2c)$^+$ system is not distributed evenly among the Au atoms (see Figure 6b), here too the majority of the excess electronic charge on the gold cluster resides on the bare 2-fold-coordinated Au atom (0.1e) with the rest divided between the two 3-fold-coordinated Au atoms (labeled 2 and 3); see Figure 8b. In contrast to the case of O_2 adsorption on the 3-fold-coordinated Au atom (Figure 6c), in the present case, adsorption on the 2-fold-coordinated Au atom (labeled 1 in Figure 8c) involves only a small excess charge localization on the adsorbed molecule (0.03e), resulting in an essentially unactivated O_2 moleule (d(O−O) = 1.28 Å), as reflected also in a relatively small value of the antibonding population estimator $S(2\pi^*)$ = 0.25.

3.2.1.2. Au_6^+ Cluster. In the ground state the atoms in the Au_6^+ cluster are arranged in a triangular (t) structure (see the top row in Figure 9) with the average distance between neighboring atoms along the edges d_{edge}(Au−Au) = 2.63 Å, and the (internal) distances between neighboring atoms vary from 2.89 Å between the two midatoms on the sides of the triangle and 2.76 Å between a midatom on the side edge and an atom at the middle of the base of the triangle (see Figure 9). The ground-state geometry of the parent neutral Au_6 cluster is also triangular with a calculated vertical ionization potential vIP = 8.11 eV and an adiabatic ionization potential aIP = 8.08 eV.

The structure of the closest higher energy (0.19 eV) isomer of the hexamer cation cluster is an incomplete hexagon (see

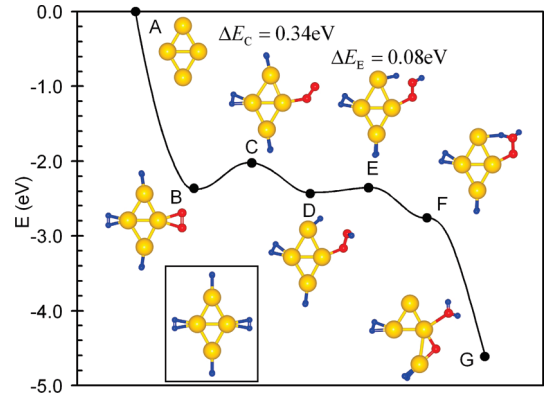

Figure 11. Profile of the reaction of H_2 and O_2 with Au_4^+ leading to dissociation of the O_2 molecule and water elimination. The reaction profile (RP) was calculated for the adsorption geometry $Au_4(H_2)_3$(3c,2c,2c)O_2(3c)$^+$, marked as configuration B (see also Figure 6c). The transition states (TSs) correspond to the configurations marked C and E, and the values of the TS barriers (read from the vertical (energy) axis) are given in the figure. Note that here, as well as in the other reaction profiles displayed below (see Figures 12−14), the reaction coordinate may correspond at various stages of the reaction to different geometrical parameters and that no distance (or angle) scale is associated with the horizontal axis of the RP. At each stage of the reaction the calculations were performed for successive variations of the selected reaction coordinate, and the configurations corresponding to (local) minima, saddle points, and (local) maxima (TS barriers), are denoted by the solid dots (accompanied by illustrations of the corresponding atomic arrangements). The hydrogen-saturated structure $Au_4(H_2)_4^+$ is shown in the inset. Au atoms are depicted by yellow balls, hydrogen atoms by blue balls, and oxygen atoms by red balls.

the top row in Figure 9), with d_{edge}(Au−Au) = 2.73 Å for the two upper Au−Au distances and d_{edge}(Au−Au) = 2.65 Å for the two lower ones, with the values for the side ones being d_{edge}(Au−Au) = 2.66 Å; the distance between the top and "middle" Au atoms is 2.77 Å. The transformation from the t to the ih structure involves an activation energy ΔE(t→ih) = 0.38 eV, and the transition-state structure is nontriangular (see the top row in Figure 9).

At saturation the triangular hexamer cation cluster binds three H_2 molecules at the apexes of the triangle with a binding energy of $E_b(3H_2^+)$ = 0.40 eV per molecule, d(H−H) = 0.80 Å, d(Au−H) = (1.91−1.96) Å (with the lower value corresponding to the top of the triangle); the average Au−Au distance after hydrogen adsorption is d_{edge}(Au−Au) = 2.68 Å (see Figure 9, middle row). This structure is essentially degenerate in energy with an incomplete hexagonal one with three H_2 molecules adsorbed to it (see Figure 9, middle row, right, where in the hydrogenated cluster the top H_2 molecule is in the plane of the gold atoms and the other H_2 molecules are normal to it). The transition between the triangular and the ih structure (with three H_2 adsorbed molecules) entails an activation barrier of 0.30 eV. In the hydrogenated triangular cluster we find an excess electronic charge on the Au atoms (see Figure 10b), with 0.076e on each of the bottom (base) Au apex atoms (labeled 4 and 6 in Figure 10c) and a charge deficiency of 0.04 on the top apex atom (labeled 1 in Figure 10 c).

For the incomplete hexagonal structure at saturation the cluster cation binds five H_2 molecules at all the apex atoms, with an average binding energy per molecule of $E_b(5H_2^+)$ = 0.38 eV (see Figure 10a); in this cluster d(Au−H) = 1.89 Å and d(H−H) = 0.81 Å. In the hydrogenated cluster there is excess electronic charge on the gold atoms with a total of 0.06e on the apex ones (distributed mainly on the atoms labeled 2, 3, 5, and 6 in Figure 10a) and 0.105e on the internal atom (labeled

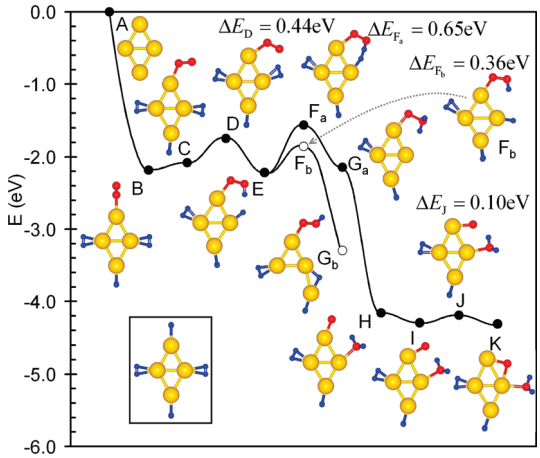

Figure 12. Profiles of the reaction of H_2 and O_2 with Au_4^+ calculated for the adsorption geometry $Au_4(H_2)_3(3c,3c,2c)O_2(2c)^+$, marked as configuration B (see also Figure 8c). One of the profiles leads to dissociation of the O_2 molecule and water elimination (the one passing through activation barrier F_a), while another one (the one passing through activation barrier F_b) does not lead to the desired product. The RP was calculated for the adsorption geometry $Au_4(H_2)_3(3c,3c,2c)O_2(2c)^+$, marked as configuration B (see also Figure 8c). The transition states encountered on the RP resulting in dissociation of the O_2 molecule correspond to the configurations marked D, F_a, and J, and the TS barriers are given in the figure. The hydrogen-saturated structure $Au_4(H_2)_4^+$ is shown in the inset. Au atoms are depicted by yellow balls, hydrogen atoms by blue balls, and oxygen atoms by red balls.

4). The fully hydrogenated $Au_6(ih)(H_2)_5^+$ cluster corresponds to the product stoichiometry $Au_6H_{10}^+$ (mass peak labeled (6,10,0)) in the experimentally measured spectrum shown in Figure 4h.

Since in the experiment oxygen adsorption was found for a cluster with three coadsorbed hydrogen molecules (see the mass peak labeled (6,6,2) in Figure 4i), we explored the adsorption of O_2 to the saturated triangular cluster, as shown in Figure 9 (bottom row). The total binding energy of the adsorbed molecules is 1.63 eV, and the adsorption energy of the O_2 molecule is 0.42 eV. The adsorbed molecule is only slightly negatively charged (0.04e), and consequently, it is only weakly activated (d(O−O) = 1.28 Å); d(Au−O) = 2.18 Å. The $Au_6(t)(H_2)_3O_2^+$ cluster may transform to a higher energy isomer (0.14 eV) with an ih structure via an activation barrier of 0.28 eV (see the bottom row in Figure 9). Instead it may transform, via a transition-state barrier of 0.38 eV, to a lower energy (0.72 eV) of ih geometry (containing a hydroperoxo group), as discussed in the context of the reaction path described in Figure 14 (transition from B_b to D).

3.2.2. Reaction Paths. In this section we focus on interactions between molecular hydrogen and oxygen that, catalyzed by gold cluster cations, lead to reactions between them. In particular, we explore reaction pathways that lead to dissociation of the oxygen molecule, starting from coadsorbed molecular hydrogen and oxygen (i.e., following a Langmuir−Hinshelwood mechanism, discussed for the reaction catalyzed by the gold tetramer and hexamer cations), as well as a case where the reaction proceeds through the interaction of preadsorbed molecular hydrogen with a gaseous oxygen molecule (that is, an Eley−Rideal mechanism, discussed as an alternative mechanism of the reaction catalyzed by the gold hexamer cation). In both cases we find that the reaction pathway involves formation of a complex containing a hydroperoxo group as a reaction intermediate. To facilitate our discussion, we present RPs, where

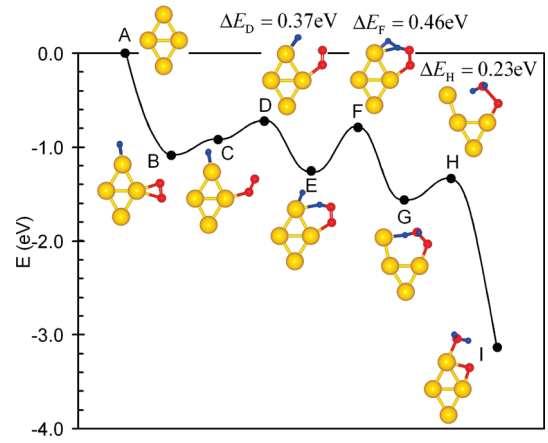

Figure 13. Profile of the reaction of H_2 and O_2 with Au_4^+ leading to dissociation of the O_2 molecule and water elimination. The RP was calculated for the adsorption geometry $Au_4H_2(2c)O_2(3c)^+$, marked as configuration B. The transition states correspond to the configurations marked D, F, and H, and the TS barriers are given in the figure. Au atoms are depicted by yellow balls, hydrogen atoms by blue balls, and oxygen atoms by red balls.

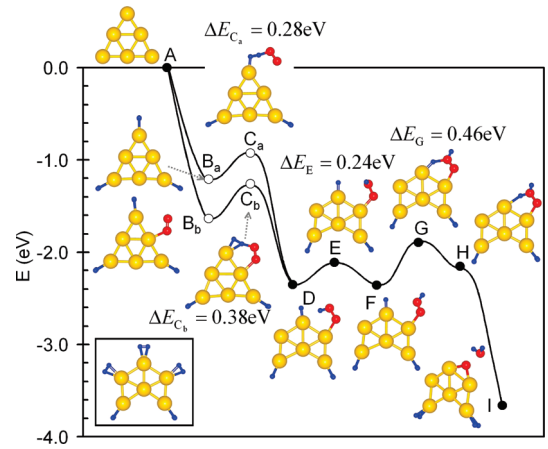

Figure 14. Profiles of the reaction of H_2 and O_2 with Au_6^+. The profile passing through the configurations marked A, B_b, C_b, D, ... correspond to a Langmuir−Hinshelwood mechanism, starting from the adsorption configuration $Au_6^+(t)(H_2)_3O_2$, marked B_b (see also the bottom row of Figures 9 and 10c). The profile passing through configurations A, B_a, C_a, D, ... correspond to an Eley−Rideal mechanism. Note that in both cases the transition from the first activation barrier encountered in the RP (C_a or C_b) to the configuration marked D involves a significant structural change, from a triangular to an incomplete hexagonal structure of the gold cluster. The other transition states encountered on the RP correspond to the configurations marked E and G; F_a and the corresponding barriers are given in the figure. The hydrogen-saturated structure $Au_6(H_2)_5^+$ is shown in the inset. Au atoms are depicted by yellow balls, hydrogen atoms by blue balls, and oxygen atoms by red balls.

we plot the variation of the energy of the reaction system along the chosen reaction coordinates and give calculated transition-state activation energies which were determined through the methodology described in section 2.3.

3.2.2.1. Reactions on Au_4^+. As shown experimentally (cf. Figure 4), adding H_2 and O_2 to the ion trap at 100 K yields the coadsorption product $Au_4H_6O_2^+$ even at a very short reaction time t_R = 0.1 s (see Figure 4, traces c and d; cf. also Figure 3), with the same coadsorption products seen for longer times and at higher temperature (200 K) (cf. traces d and e in Figure 4). Corresponding calculated configurations (marked B) are shown in Figures 11 and 12 and have been discussed by us above (see Figures 6c and 8c). For both of the O_2 adsorption sites (i.e.,

2-fold- and 3-fold-coordinated Au atoms) we find a well-bound O_2 molecule (with adsorption of the molecule being barrier free) that is activated close to a superoxo state when bound to a 3-fold-coordinated Au atom (bond length d(O−O; $Au_4(H_2)_3O_2(3c)^+$) = 1.33 Å in Figures 6c and 11, configuration B). When the trap is heated to 200 K, $Au_4H_4^+$ is detected instead of the saturation hydrogen coverage $Au_4H_8^+$ (see trace d in Figure 4); the calculated total energy difference between the ground-state energies of $Au_4H_4^+$ and $Au_4H_8^+$ ranges between 1.28 and 0.95 eV, depending on the H_2 adsorption sites (see Table 1).

Only when the temperature is increased to 300 K do we observe new products. Indeed, at this temperature one observes in addition to the bare Au_4^+ signal a new mass peak corresponding to the mass of $Au_4H_2O^+$ containing a single oxygen atom, with the mass peak corresponding to $Au_4H_6O_2^+$ disappearing, reflecting the dissociation of the initially coadsorbed O_2 molecule. Reaction profiles, starting from the two adsorption geometries of the O_2 molecule, are shown in Figures 11 and 12, with an additional RP, corresponding to O_2 adsorption at the Au(3c) site (as in Figure 11), but with only a single coadsorbed H_2 molecule, displayed in Figure 13 (this case has not been observed experimentally). The calculated reaction profiles in Figures 11−13 reveal the microscopic mechanism of the reaction starting from the ground state of $Au_4H_6O_2^+$ (B). In Figure 11 a TS energy barrier (ΔE_c = 0.34 eV) is encountered in taking the system from configuration B to the TS configuration (C, where d(O−O) = 1.28 Å), which relaxes to the hydroperoxo (−OOH) configuration marked D in Figure 11 (in this configuration d(O−O) = 1.41 Å and d(O−H) = 0.99 Å). Traversing a subsequent small TS barrier (ΔE_E = 0.08 eV), the system relaxes to a configuration G with a weakly adsorbed H_2O molecule, whose removal entails an energy of 0.40 eV, resulting in $Au_4H_4O^+$. Removal of the H_2 molecule (bonded to the left corner of the gold triangle in G) requires an additional 0.61 eV, thus obtaining $Au_4H_2O^+$, which can be identified with the mass peak labeled (4,2,1) in the experimentally measured mass spectrum (Figure 4f).

Starting from configuration B in Figure 12, corresponding to a slightly activated coadsorbed oxygen molecule anchored to a gold cluster cation at a Au(2c) site, formation of the hydroperoxo intermediate (configuration E in Figure 12) requires a larger TS barrier, ΔE_D = 0.44 eV. An even larger TS barrier, ΔE_{Fa} = 0.65 eV, is encountered toward the eventual formation of an adsorbed water molecule and a single adsorbed oxygen atom (configuration K in Figure 12). The energy required for the water molecule elimination is 0.63 eV, and an additional 0.46 eV is required for desorption of the (bottom) H_2 molecule, resulting in formation of the aforementioned $Au_4H_2O^+$ product; the energy liberated in the transition from G_a to H is sufficient for the desorption of both the H_2O and H_2 molecules. We also included in Figure 12 a reaction path that does not lead to formation of an adsorbed water molecule and does not yield the desired product (see the path E → F_b → G_b, involving a barrier ΔE_{Fb} = 0.36 eV).

To illustrate the dependence of the RP of the oxygen molecule on the hydrogen coverage, we display in Figure 13 the RP for a single coadsorbed H_2 molecule, starting from configuration B ($E_b(O_2)$ = 0.50 eV, d(O−O) = 1.32 Å) of the $Au_4H_2(2c)O_2(3c)^+$ cluster. Here we encounter a succession of two TS barriers, $\Delta E_{B\rightarrow C}$ = 0.17 eV and $\Delta E_{C\rightarrow D}$ = 0.20 eV (or in a combined form ΔE_D = 0.37 eV) with d(Au−O) = 2.22 Å, d(O−O) = 1.28 Å, and d(O−H) = 2.475 Å at TS configuration D. Relaxation from the TS leads to formation of a hydroperoxo intermediate E, with d(O−O) = 1.36 Å and d(O−H) = 1.03 Å. The hydroperoxo group transforms through a higher activation barrier (ΔE_F = 0.46 eV) to a H_2O−O− intermediate G, which leads to formation of an adsorbed water molecule and an adsorbed single oxygen atom (configuration I) through an additional TS barrier ΔE_H = 0.23 eV. Removal of the adsorbed H_2O molecule requires an energy of 0.735 eV (which is readily available from the energy liberated in the transition from H to I). Altogether, the prohibitive complexity of the reaction mechanism and the relatively large multiple activation energy barriers encountered in the reaction involving a single coadsorbed H_2 molecule (Figure 13), in comparison with the relatively simple and facile reaction profile corresponding to the reaction of adsorbed O_2 in the presence of three coadsorbed H_2 molecules as displayed in Figure 11, serve to illustrate the promoting effect of the increased coverage of coadsorbed hydrogen on the dissociation reaction of an adsorbed oxygen molecule on gold tetramer cation clusters (Figure 11).

3.2.2.2. Reactions on Au_6^+. When the gold hexamer cation interacts at 100 K with hydrogen only, a saturated species with five H_2 molecules per cluster is observed (see mass peak labeled (6,10,0) in Figure 4h corresponding to an incomplete hexagonal structure of $Au_6(H_2)_5^+$, shown in Figure 10a and in the inset of Figure 14). However, when both O_2 and H_2 are admitted to the trap at 100 K, the coadsorption product labeled (6,6,2) in the mass spectrum shown in Figure 4i, corresponding to the triangular structure of $Au_6(t)(H_2)_3O_2^+$, is the sole mass signal found (cf. the bottom row of Figure 9, Figure 10c, and configuration B_b in Figure 14), where the total binding energy of the three H_2 molecules is 1.21 eV and that of the coadsorbed O_2 molecule is 0.42 eV. As aforementioned, the activation and dissociation of the coadsorbed oxygen molecule with increasing temperature is even more apparent for the Au_6^+ cluster than for the gold tetramer cation discussed above. Indeed, trace k in Figure 4, obtained at an increased reaction time of 2.0 s and 200 K, reveals that already at this relatively low temperature an additional mass peak corresponding to a dissociated oxygen species (labeled (6,4,1)) emerges (while for the gold tetramer oxygen dissociation required heating to 300 K; see Figure 4f).

The RP, starting from the coadsorption ground-state configuration B_b, is shown in Figure 14, exhibiting a Langmuir−Hinshelwood mechanism. We find that the triangular-shaped ground-state gold cluster cation transforms to an incomplete hexagonal geometry with a hydroperoxo group (see D in Figure 14) through a TS activation barrier ΔE_{Cb} = 0.38 eV; in the TS configuration C_b d(O−O) = 1.30 Å and the distance between the closest O and H atoms is d(O−H) = 1.40 Å. The gain in energy in transforming from the TS to the hydroperoxo intermediate (configuration D) is 0.72 eV, and in D d(O−O) = 1.37 Å and d(O−H) = 1.03 Å. The energy required to remove one of the bottom hydrogen molecules from configuration D is 0.53 eV, leaving a cluster with a nuclearity of $Au_6(H_2)_2O_2^+$ corresponding to the mass peak labeled (6,4,2) in the experimental spectra shown in Figure 4j,k.

Subsequently, we find two TS barriers: one for rotation of the hydroperoxo group (configuration F) with a barrier ΔE_E = 0.24 eV and the other for forming the complex marked H which entails a barrier of ΔE_G = 0.46 eV. Subsequent relaxation leads to water elimination ending with $Au_6H_4O^+$ (configuration I) containing a dissociated, single, adsorbed oxygen atom. This final configuration corresponds to the mass peak labeled (6,4,1) in the measured mass spectra in Figure 4k,l. We note that, in

agreement with the experiments, the O_2 dissociation reaction for the Au_6^+ cluster is predicted to entail smaller activation barriers than in the Au_4^+ case, and is thus expected to occur at a lower temperature, as is indeed observed; as aforementioned, $Au_xH_yO^+$ products are detected already at 200 K for Au_6^+, but only at 300 K for Au_4^+.

Up to this point all the reaction mechanisms that we discussed were of the Langmuir−Hinshelwood (LH) type, starting from reactants (hydrogen and oxygen molecules) coadsorbed on the gold cluster cation. We close with a discussion of an alternative reaction mechanism for the reaction on the gold hexamer cation, which is of the Eley−Rideal (ER) type, indicated by the path $A \rightarrow B_a \rightarrow C_a \rightarrow D \rightarrow ...$ in Figure 14. In this mechanism we start from the hydrogen-saturated triangular structure of the $Au_6(H_2)_3^+$ cluster (B_a, with the total binding energy of the H_2 molecules being 1.21 eV). A gaseous O_2 molecule binds to the cluster through a TS barrier $\Delta E_{Ca} = 0.28$ eV; see the TS configuration labeled C_a, where the inter-hydrogen atom distance in the molecule involved in the reaction d(H−H) = 0.96 Å, d(O−O) = 1.28 Å, and d(O−H) = 1.35 Å. Relaxation from the TS transforms the gold cluster to an incomplete hexagonal structure and results in formation of a hydroperoxo intermediate (configuration D, discussed above for the LH mechanism). Subsequent steps of the reaction leading to oxygen dissociation and water elimination are the same as those discussed above for the LH mechanism.

4. Summary

In this paper we presented a joint experimental and theoretical study where we have explored the characteristics and factors that control the cooperative coadsorption of hydrogen and oxygen on cationic gold clusters Au_x^+ ($x = 2 - 7$), with a particular emphasis on Au_4^+ and Au_6^+. Product ion mass distributions were obtained in an octopole ion trap under multicollision conditions at temperatures of 300, 200, and 100 K as well as for ion storage times $t_R = 0.1-2$ s. The temperature-dependent reactions of the clusters exposed to solely hydrogen revealed a strictly negative temperature dependence and thus a barrier-free hydrogen chemisorption with saturation coverages of H_2 molecules corresponding to the number of corner sites in the ground-state structures of the clusters (except for Au_2^+ where the hydrogen saturation coverage of three H_2 exceeds the number of corners; see Figure 2). In contrast, temperature-dependent measurements for Au_4^+ and Au_6^+ yield a negative temperature dependence for $Au_xH_yO_2^+$ products, but a positive temperature dependence for $Au_xH_yO^+$, indicating the presence of an activation barrier in the latter case.

First-principles calculations, based on density-functional theory, provided a detailed picture of the nature of the adsorption of H_2 and O_2 to cationic gold clusters. Bonding of H_2 molecules to the cluster cations was found to involve the transfer of charge from the molecules to the gold atoms. The calculated saturation coverages agree with the experimental ones (four H_2 molecules and five H_2 molecules for Au_4^+ and Au_6^+, respectively; see Figures 2, 4, 6, 8, and 10). For the case of Au_6^+, the ground-state structure was determined to have a triangular atomic arrangement and a higher energy isomer (0.19 eV) with an incomplete hexagonal (ih) structure was found (Figure 9). At saturation coverage of the triangular structure (that is, the adsorption of three H_2 molecules) the triangular and ih isomer ($Au_6(ih)(H_2)_3^+$) are found to become degenerate in energy, and the transformation between these structures upon adsorption (termed also "structural fluctionality") was determined to involve a barrier of 0.30 eV (see Figure 9); a similar barrier separates the two isomers with coadsorbed three H_2 molecules and one O_2 molecule (see the bottom row of Figure 9).

The coadsorption of O_2 was found to entail occupation of the antibonding $2\pi^*$ orbitals of the molecule (see the analysis in Figure 7), resulting in excess electronic charge accumulation on the adsorbed molecule (see Figures 6, 8, and 10), with a consequent weakening of the O−O bond, and activation of the adsorbed molecule.

Theoretical investigations of the evolution of the reaction along the reaction coordinate allowed elucidation of the dynamics and microscopic mechanisms and determination of reaction profiles and activation barriers. The measurements (see Figure 4) and the theoretical analysis (see Figures 11−14) revealed that the promotion and activation of molecular oxygen by hydrogen preadsorption leads to the formation of a hydroperoxo intermediate on Au_4^+ and Au_6^+, culminating with the dissociation of O_2 via the release of H_2O. Langmuir−Hinshelwood reaction mechanisms involving the coadsorption of both of the reactant molecules were discussed for both cluster sizes (Figures 11−14), and an alternative Eley−Rideal mechanism involving hydrogen molecules adsorbed on a Au_6^+ cluster reacting with an impinging gaseous oxygen molecule (see Figure 14) was analyzed.

The theoretical results for saturation coverages and reaction characteristics were found to agree with the experimental findings. The joint investigations provide useful insights regarding hydrogen and oxygen cooperative adsorption effects and consequent reaction mechanisms. In particular, the current findings guide our ongoing analysis pertaining to selective hydrocarbon oxidation by molecular oxygen on free and supported gold particles, in which hydrogen preadsorption is found to be required to achieve an efficient and highly selective process.

Acknowledgment. Financial support by the Deutsche Forschungsgemeinschaft and the Fonds der Chemischen Industrie is gratefully acknowledged. S.M.L. thanks the Fonds der Chemischen Industrie in particular for a Kekulé fellowship. The theoretical work (R.N.B., B.Y., and U.L.) was supported by the U.S. Department of Energy, the Air Force Office for Scientific Research, and the NSF. Calculations were performed at NERSC, Berkeley, CA, the DOD supercomputer center, and the Georgia Tech Center for Computational Materials Science.

JA9022368